Petroleum 9 (2023) 412–418

Contents lists available at ScienceDirect

Petroleum

journal homepage: www.keaipublishing.com/en/journals/petlm

Geostress effect on resistivity and its relevant correction method

Hongquan Xia , Shuxian Jiang *

State Key Laboratory of Oil & Gas Reservoir Geology and Exploitation, Southwest Petroleum University, Chengdu, 610500, China

ARTICLE INFO

Article history:
Received 12 August 2020
Received in revised form
19 April 2021
Accepted 22 June 2021

Keywords:
Resistivity correction
Reservoir fluid identification
Effect of geostress

ABSTRACT

For reservoirs with abnormally high pressure and high geostress, formation resistivity can be greatly affected. This increase of resistivity resulting from high stress causes errors in the identification of reservoir fluids. In order to investigate the effect of stress on resistivity, resistivity measurement was conducted simultaneously with triaxial testing to obtain rock resistivity under high temperature and high pressure. The changes of resistivity and resistivity increasing coefficient with horizontal differential stress and minimum horizontal stress were revealed from experiments. Besides, field data were analyzed to show the main influencing factors of formation resistivity under reservoir conditions. In addition, a new resistivity correction model for high geostress formation was derived in this work. The interpretation results are in good agreement with well testing data in the Keshen area of the Tarim oilfield, China.

1. Introduction

In order to investigate the effect of stress on resistivity, researchers designed experiments to measure resistivity under different stress conditions. Glanville [1] revealed that resistivity is influenced by the difference of overburden and fluid pressure. This influence varies with porosity, lithology and water saturation. Experiments were performed to measure the resistivity of samples with different lithologies, including sandstone and carbonate rocks under uniaxial stress conditions or triaxial stress conditions [2–6]. The effect of pressure, temperature, and saturation on resistivity were studied through experiments [7–10]. Results showed that resistivity measurement is closely related to stress conditions and fluid saturation. Wang et al. [11] designed experiments and investigated the stress effect on resistivity. It was revealed that resistivity increased with stress and the changes in resistivity was related to the direction of measurement. Liu et al. [12] studied the relationship between resistivity and horizontal stress difference. A flow chart for resistivity correction was raised, but the calculation process was relatively complex.

The relationships between resistivity and stress were also derived with numerical or analytic methods. The effect of stress on pore structure is the main reason for the considerable increase in resistivity. Other influencing factors such as effect of formation dip angles or layered rocks on resistivity were also investigated through numerical methods [13,14]. Porosity is one of the most important factors affecting resistivity. Perez-Rosales [15,16] developed the relationship between resistivity factor and porosity with an analytical solution and pointed out that the cementation exponent in the Archie equation has a great significance to resistivity. Küntz et al. [17] gave numerical estimates of formation factor as a function of porosity for various pore geometries. Verwer et al. [18] showed that pore structure and the number of pores are controlling factors of carbonate resistivity. Li et al. [19] analyzed the influence of pore geometry on formation resistivity factor in sandstone formations. In addition to pores, researchers also studied the effect of throats geometry and fractures on resistivity [20,21].

In this study, the research area is located in the Keshen play of the Tarim oilfield. The Cretaceous Bashijiqike Formation of the Keshen area is a low-porosity, low-permeability sandstone reservoir and the average burial depth is over 6000 m. An abnormal increase in resistivity was observed due to high geostress. Geostress values are mainly achieved in two ways for this research. Through hydraulic fracturing method, the minimum horizontal stress and fracturing pressure can be identified. In addition, some geostress

* Corresponding author.
E-mail address: sxjiang@swpu.edu.cn (S. Jiang).
Peer review under responsibility of Southwest Petroleum University.

Production and Hosting by Elsevier on behalf of KeAi

https://doi.org/10.1016/j.petlm.2021.06.003

values are calculated according to acoustic and electric imaging log data and wellbore caving features. High geostress leads to errors when estimating water saturation and fluid types with the abnormally high resistivity. To solve this problem, the effect of geostress on resistivity was analyzed in this study. Based on the experimental results and field data, a new resistivity correction model considering the effect of stress was raised. A good agreement between the fluid identification based on the proposed model and well testing results was observed in the research area.

2. Experimental design

Samples were obtained from Bashijiqike Formation outcrop and processed into uniform cores whose specifications were 5 cm× 5 cm× 5 cm. These samples are mainly composed of medium-grained lithic sandstone. To simulate the formation water with high salinity in the research area, samples were vacuumed until fully saturated with 18% NaCl solution.

Resistance was measured with a ZL5 intelligent LCR meter. Inside the meter, a squared core holder can provide high pressure and high temperature. Samples were placed in the core holder and stress was provided in three directions. The measurement of rock resistivity is shown in Fig. 1. The resistivity of samples was measured in the X direction at 90 °C. The resistivity of samples can be calculated with Eq. (1).

$$R_t = \frac{rs}{100L} \tag{1}$$

where R_t is resistivity of rock samples, Ω.m;
r is resistance of rock samples, Ω;
s is cross section area of samples, cm^2;
L is length of rock samples, cm.

According to the stress conditions of the Keshen area, target stratums can be divided into extension section and compress-shear section. Thus in the experiment, two types of stress conditions were applied. The first type is that the axial stress is higher than the confining stress. This type is to simulate the stress condition that the overburden stress is equal to the minimum horizontal stress. The second one is the axial stress is lower than the confining stress, which simulate the stress condition that the overburden stress is equal to the maximum horizontal stress.

Accordingly, two types of testing procedures were applied in the experiment. One type is that the axial stress is increased to 70 MPa in increments of 10 MPa under a fixed confining stress in each cycle.

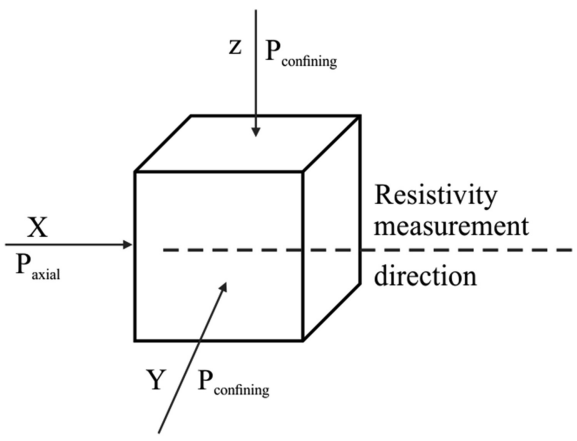

Fig. 1. Schematic diagram of resistivity measurement.

The confining stress is lower than the axial stress and is set 10 MPa, 20 MPa, 30 MPa, 40 MPa, 50 MPa and 60 MPa in different cycles. The other type is that the confining stress is increased to 70 MPa in increments of 10 MPa under a fixed axial stress in each cycle. The axial stress is lower than the confining stress and is set 10 MPa, 20 MPa, 30 MPa, 40 MPa, 50 MPa and 60 MPa in different cycles.

3. Results

Through experiments, the relationship between resistivity and horizontal differential stress (the difference between axial stress and confining stress) under different minimum horizontal stresses can be achieved. As shown in Fig. 2a, when the axial stress is higher than the confining stress, measured resistivity increases with horizontal differential stress when the minimum horizontal stress is fixed. The exponential increase is obvious when enough data points are collected in each cycle. Besides, the effect of minimum horizontal stress on measured resistivity is not significant under a fixed horizontal differential stress.

Fig. 2b demonstrates the changes in resistivity with horizontal differential stress under different minimum horizontal stresses when the confining stress is higher than the axial stress. Resistivity increases exponentially with horizontal differential stress under a fixed minimum horizontal stress. The increment of resistivity decrease with horizontal differential stress. Moreover, resistivity increases with the minimum horizontal stress when the horizontal differential stress maintains the same.

To show the effect of stress on resistivity, a stress-resistivity increasing coefficient ($I_{es} = \frac{R_t}{R_0}$) is introduced. R_0 and R_t indicate resistivity values of samples before and after axial stress is applied under different confining stress conditions. The variations of resistivity and resistivity increasing coefficient with the horizontal differential stress and the minimum horizontal stress are summarized in Table A, B and C in Appendix. It can be seen that the resistivity increasing coefficient of samples increases exponentially with horizontal differential stress and the minimum horizontal stress.

4. The effect of geostress on resistivity

4.1. The correlation between resistivity and vertical effective stress

With the development of oil and gas fields, pore pressure decreases and effective stress increases, causing closer particle arrangement and smaller pore volume. As the vertical effective stress increases, cementation exponent increases and the pore throat diameter decreases sharply, resulting in the decrease of the ionic conductive capability of formation fluids. Fig. 3 presents the relationship between formation resistivity and the vertical effective stress in ks5 well in the research area. It can be seen that formation resistivity increases exponentially with vertical effective stress.

4.2. The correlation between resistivity and horizontal differential stress

Along with the increase of horizontal differential stress, the lateral compaction of rock becomes stronger and the rock porosity decreases linearly. Because of the smaller pore size and slower ion movement, formation resistivity increases exponentially with horizontal differential stress (Fig. 4). Since the lateral tectonic compression is strong in the Keshen area, the exponential increase of resistivity with horizontal differential stress is common in the wells of this area.

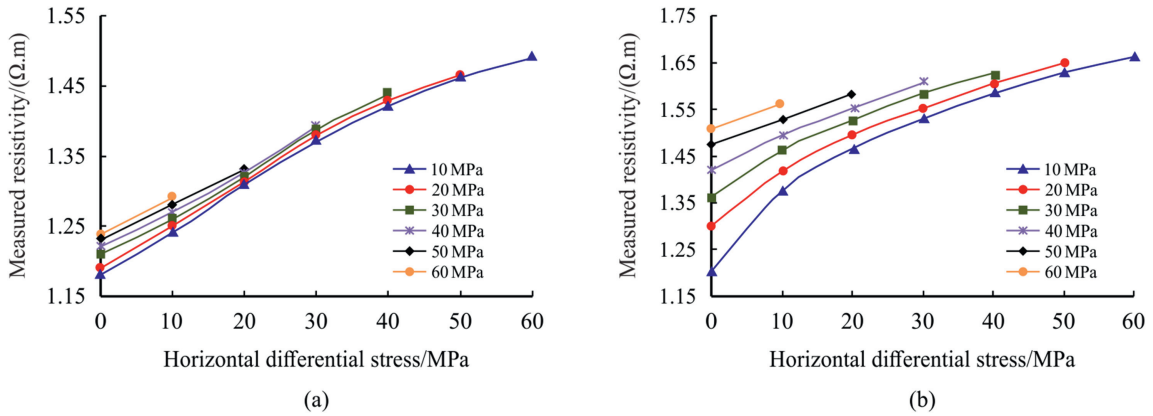

Fig. 2. The variation of resistivity with horizontal differential stress under different groups of minimum horizontal stress. (a) Resistivity measurement when axial stress is higher than confining stress; (b) Resistivity measurement when confining stress is higher than axial stress.

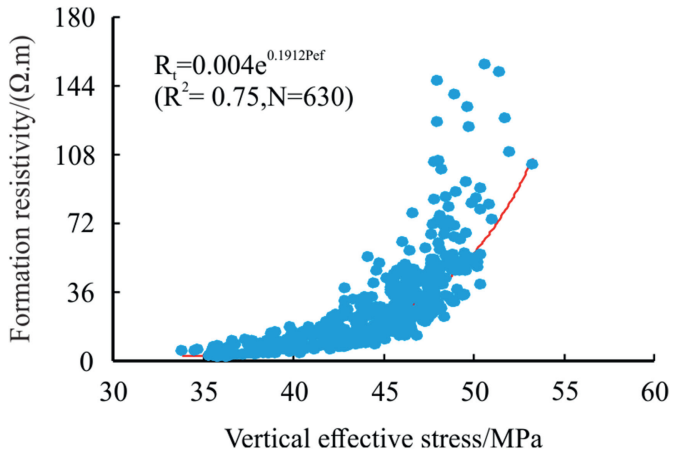

Fig. 3. The relationship between formation resistivity and effective stress in ks5 well in the research area.

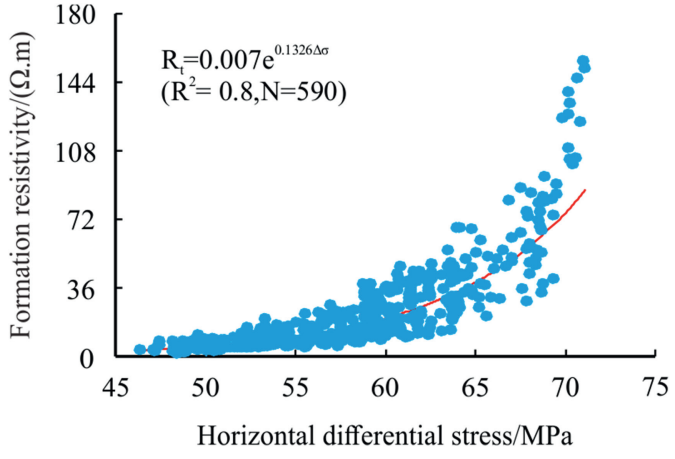

Fig. 4. The relationship between formation resistivity and horizontal differential stress in ks5 well in the research area.

4.3. The correlation between resistivity and side-pressure coefficient

Normally, side-pressure coefficient ($K = (\sigma_H + \sigma_h)/ 2\sigma_V$) is the ratio of the average of two horizontal stresses and the vertical stress. However, the range of the K value is large and the changes cannot reflect the influence of the principal stresses on formation resistivity. So an improved side-pressure coefficient $K' = (\sigma_H - \sigma_h)/(P_0 - \alpha P_p)$ is introduced to show the roles of differential stress in the horizontal direction and the effective stress in the vertical direction. The lateral and vertical compaction reduces formation porosity markedly, resulting in the increase of the cementation exponent and formation resistivity. As shown in Fig. 5, formation resistivity increases exponentially with side-pressure coefficient K' in ks5 well in the research area.

From resistivity experiments, it can be found that resistivity increases exponentially with minimum horizontal stress and differential stress. According to data from oilfields, formation resistivity increases exponentially with horizontal differential stress, effective stress, and side-pressure coefficient. Based on the relationships between resistivity and stress that are achieved from both experiments and field data, a new resistivity correction model was proposed.

5. A new resistivity correction model

According to the experimental results and field data analysis, stress-resistivity increasing coefficient increases exponentially with horizontal differential stress and effective stress. The relationships are expressed in Eq. (2) and Eq. (3).

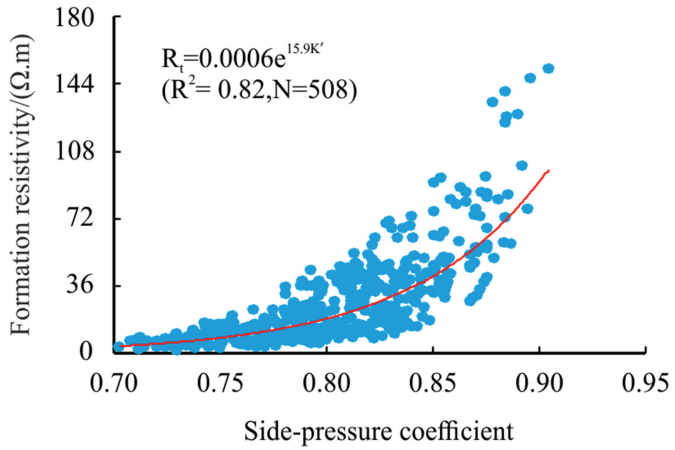

Fig. 5. The relationship between formation resistivity and side-pressure coefficient K' in ks5 well in the research area.

Table 1
Log interpretation based on resistivity correction model for ks503 well at the depth interval of 6844m–7049 m (D_t: top depth of layers; D_b: bottom depth of layers; ϕ: porosity; R_{bc}: resistivity before correction; R_{ac}: resistivity after correction; Result 1: fluid identification with resistivity before correction; Result 2: fluid identification with resistivity after correction).

#NO	D_t (m)	D_b (m)	σ_H (MPa)	σ_h (MPa)	$\Delta\sigma$ (MPa)	P_{ef} (MPa)	ϕ (%)	R_{bc} ($\Omega \cdot m$)	R_{ac} ($\Omega \cdot m$)	Result 1	Result 2
1	6844	6845	198.78	139.99	58.80	43.13	5.07	19.97	17.48	Gas layer	Gas layer
2	6846	6855	196.84	138.08	58.76	43.62	5.54	14.55	12.72	Gas layer	Gas layer
3	6856	6857	194.29	136.54	57.75	43.41	5.14	18.87	16.53	Gas layer	Gas layer
4	6858	6866	200.43	141.13	59.30	41.51	4.94	12.52	10.96	Gas layer	Gas layer
5	6868	6871	207.22	147.79	59.43	44.67	5.82	22.56	19.50	Gas layer	Gas layer
6	6876	6880	198.82	138.24	60.58	46.08	4.94	26.15	22.72	Gas layer	Gas layer
7	6882	6887	207.94	146.44	61.50	39.63	5.41	7.98	6.97	Gas layer	Gas layer
8	6887	6889	202.63	142.70	59.93	42.51	5.27	19.93	17.42	Gas layer	Gas layer
9	6890	6892	205.07	144.41	60.66	38.12	5.48	7.65	6.69	Gas layer	Gas layer
10	6892	6894	206.33	145.30	61.03	39.75	5.86	9.99	8.73	Gas layer	Gas layer
11	6894	6897	204.91	144.11	60.80	42.46	5.11	12.66	11.04	Gas layer	Gas layer
12	6897	6900	204.17	143.79	60.38	39.87	6.21	12.27	10.73	Gas layer	Gas layer
13	6901	6903	203.11	143.17	59.94	44.94	4.53	13.01	11.29	Gas layer	Gas layer
14	6905	6914	203.60	144.63	58.97	42.42	4.97	14.98	10.02	Gas layer	Gas layer
15	6917	6924	204.32	141.54	62.78	44.19	4.63	29.19	19.48	Water-bearing gas layer	Gas -bearing water layer
16	6934	6937	208.52	146.28	62.24	44.06	4.54	24.69	16.40	Water-bearing gas layer	Gas -bearing water layer
17	6938	6940	208.38	144.39	63.99	45.52	4.55	29.77	19.75	Water-bearing gas layer	Gas -bearing water layer
18	6940	6949	203.53	141.15	62.38	41.45	4.34	27.30	18.29	Water-bearing gas layer	Gas -bearing water layer
19	6949	6951	209.57	144.90	64.67	44.57	3.85	43.65	27.62	Water-bearing gas layer	Gas -bearing water layer
20	6960	6965	205.44	143.44	62.00	44.62	4.92	22.26	7.71	Gas layer	Water-bearing gas layer
21	6966	6967	209.66	146.10	63.56	45.91	4.04	30.52	10.04	Gas layer	Water-bearing gas layer
22	6968	6969	207.88	146.14	61.74	43.59	4.57	26.42	11.52	Gas layer	Gas -bearing water layer
23	6975	6977	209.00	145.46	63.54	42.58	4.92	17.79	7.79	Gas layer	Water-bearing gas layer
24	6978	6980	207.71	144.24	63.47	46.39	4.14	26.83	11.02	Gas layer	Water-bearing gas layer
25	6983	6987	202.30	140.03	62.27	45.68	4.41	26.79	10.67	Gas layer	Water-bearing gas layer
26	6994	7001	205.36	142.57	62.80	44.17	4.14	20.34	7.51	Gas layer	Water-bearing gas layer
27	7007	7013	211.90	147.92	63.98	45.35	4.15	34.03	11.93	Gas layer	Water-bearing gas layer
28	7016	7022	222.50	154.23	68.27	50.30	2.23	90.23	27.92	Dry layer	Dry layer
29	7023	7025	211.08	145.71	65.37	47.33	2.84	81.86	25.78	Dry layer	Dry layer
30	7026	7030	216.19	148.95	67.24	48.05	3.73	65.11	20.33	Dry layer	Dry layer
31	7030	7032	220.35	152.92	67.43	46.42	2.93	56.53	17.66	Dry layer	Dry layer
32	7035	7040	218.34	150.25	68.09	48.16	3.23	76.82	23.93	Dry layer	Dry layer
33	7041	7049	212.66	145.80	66.86	47.99	2.95	72.24	22.70	Dry layer	Dry layer

$$I_{es} = \frac{R_t}{R_0} = a \times e^{b \times \Delta\sigma} \tag{2}$$

$$I_{es} = \frac{R_t}{R_0} = c \times e^{d \times \sigma_h} \tag{3}$$

Eq. (2) and Eq. (3) can be rearranged as:

$$Ln(\ I_{es}) = Ln(a) + b \times \Delta\sigma \tag{4}$$

$$Ln(\ I_{es}) = Ln(c) + d \times \sigma_h \tag{5}$$

It can be seen from Eqs. (4) and (5) that $Ln(\frac{R_t}{R_0})$ is a function of $\Delta\sigma$ and σ_h. Since side pressure coefficient K' ($\frac{\Delta\sigma}{P_{ef}}$) also has a great impact on I_{es}, K' can be introduced into the $Ln(\frac{R_t}{R_0})$function.

$$Ln(\ I_{es}) = f(\Delta\sigma, \sigma_h, \frac{\Delta\sigma}{P_{ef}}) \tag{6}$$

Using multivariate linear analysis, Eq. (7) can be achieved based on resistivity data under different groups of horizontal differential stress, effective stress and side pressure coefficient in the experiment.

$$Ln(I_{es}) = m\ \Delta\sigma + n\sigma_h + x\frac{\Delta\sigma}{P_{ef}} + y \tag{7}$$

The stress-resistivity increasing coefficient can be calculated as:

$$I_{es} = e^{m\ \Delta\sigma + n\sigma_h + x\frac{\Delta\sigma}{P_{ef}} + y} \tag{8}$$

The reciprocal of stress-resistivity increasing coefficient and multiplication coefficient I_C are applied to calibrate the measured resistivity. The resistivity correction equation can be expressed as:

$$R_{tsc} = \frac{R_t}{I_C \times I_{es}} \tag{9}$$

By substituting Eq. (8) into Eq. (9), the corrected resistivity can be calculated as:

$$R_{tsc} = R_t \Big/ (I_C \times e^{m\ \Delta\sigma + n\sigma_h + x\frac{\Delta\sigma}{P_{ef}} + y}) \tag{10}$$

6. Validation of resistivity correction model

Before we make resistivity correction considering geostress, we have finished mud-filtrate invasion correction, borehole correction and formation anisotropy correction to eliminate the influence of other factors. Since the Keshen area is under abnormally high pressure and strong tectonic stress, geostress has a significant impact on formation resistivity. The high stress in the target intervals causes an abnormal increase in resistivity. So it is hard to identify fluid types based on traditional methods. For instance, some layers with high resistivity were interpreted as gas layers, but well testing results show that these layers are water layers.

In this study, the reservoir in the research area changes from extension section to compress-shear section from shallow to deep depth. According to the experimental results of resistivity under different groups of horizontal differential stress, effective stress and side pressure coefficient, the stress-resistivity increasing coefficient for different zones are expressed as:

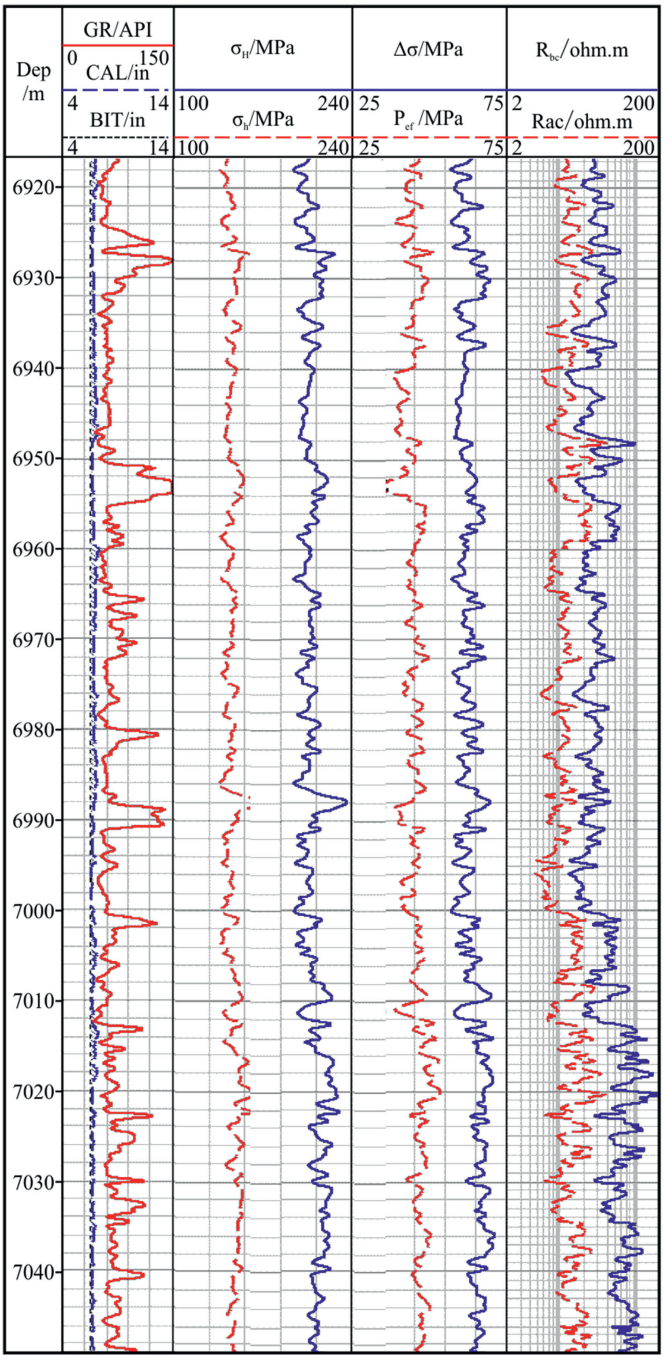

Fig. 6. Resistivity correction results in ks5 well at the depth interval of 6920m–7049 m

Extension section:

$$Ln(I_{es1}) = 0.003852\Delta\sigma + 0.000473\sigma_h + 0.003212\frac{\Delta\sigma}{P_{ef}} + 0.021735 \quad (11)$$

Compress-shear section:

$$Ln(\mathrm{I}_{es2}) = 0.002941\Delta\sigma + 0.001061\sigma_h + 0.021109\frac{\Delta\sigma}{P_{ef}} + 0.057014 \quad (12)$$

Through Eqs. 10–12, corrected resistivity considering the effect of stress can be calculated. The multiplication coefficient I_C may vary from different plays. Resistivity correction of wells in the Keshen area was made based on the proposed stress-resistivity correction model. Firstly, Stress such as overburden stress, pore pressure, and horizontal stress was calculated based on well log data. Water/gas saturation was calculated with the corrected resistivity. The fluid identification results based on the resistivity correction model were compared with well testing results. These comparison results provide a basis for the stress-resistivity correction process of new wells.

KS503 well in the research area has small caliper variations and the formation is mainly composed of fine sandstone, so the impact of caliper and lithology on resistivity can be neglected. As shown in Table 1, in the depth interval of 6844 m to 6914 m, $\Delta\sigma$ has an average value of 59.85 MPa, P_{ef} has an average value of 42.29 MPa, ϕ has an average value of 5.31% and average resistivity value before correction is 15.22 Ω·m. In the depth interval of 6914 m to 7013 m, $\Delta\sigma$ has an average value of 63.03 MPa, P_{ef} has an average value of 44.47 MPa, ϕ has an average value of 4.40% and average resistivity value before correction is 27.66 Ω·m. In the depth interval of 7013 m to 7048 m, $\Delta\sigma$ has an average value of 67.21 MPa, P_{ef} has an average value of 48.04 MPa, ϕ has an average value of 2.99% and average resistivity value before correction is 73.80 Ω·m. The well testing results indicate that water production is 150 m^3 in the interval of 6960 m to 7013 m. But calculated gas saturation based on resistivity show that this interval is a gas layer.

With the resistivity correction model, the average resistivity value at the depth interval of 6844 m to 6914 m is 13.06 Ω·m, which is 14.2% lower than resistivity before correction. The average resistivity value at the depth interval of 6914 m to 7013 m is 13.83 Ω·m, which is 50.0% lower than resistivity before correction. At the depth interval of 6845 m to 6872 m, the values of gas saturation calculated based on resistivity before and after correction are 59.66% and 57.16%, respectively. The interpretation results are gas layers based on these two saturation values. At the depth interval of 6960 m to 7013 m, the values of gas saturation calculated based on resistivity before and after correction are 57.91%, 37.96%, respectively. The interpretation results are changed from gas layers to water-bearing gas layers. Well testing results show that gas production is 188938 m^3 per day at the depth interval of 6844 m to 6871 m and water production is 150 m^3 per day at the depth interval of 6960 m to 7013 m. Therefore, the gas saturation results calculated with the corrected resistivity are in good agreement with well testing results.

In order to show geostress effect on resistivity, the resistivity results before and after using correction model are shown in Fig. 6. In this figure, track 1 includes Gamma Ray log, caliper log and bit size. Track 2 and Track 3 show geostress factors including the maximum horizontal stress, the minimum horizontal stress, horizontal differential stress and vertical effective stress. The last track indicates the difference between resistivity values before and after correction.

7. Conclusions

A novel resistivity correction model considering the effect of stress was proposed in this study. The following conclusions can be drawn on the basis of the experiment analysis, model derivation and validation.

(1) Simultaneous resistivity measurement and triaxial testing reveal that rock resistivity increases exponentially with horizontal differential stress and the minimum horizontal stress.

(2) Field data show that resistivity increases exponentially with vertical effective stress, horizontal differential stress, and side-pressure coefficient, which are important factors influencing formation resistivity.
(3) The results calculated with the proposed resistivity correction model are in good agreement with well testing data in the Keshen area of the Tarim oilfield, China. The gas saturation values calculated with the corrected resistivity provide more accurate fluid identification results than with uncorrected resistivity.

Acknowledgements

The authors would like to acknowledge China Petroleum logging Co. for providing the logging data used in the study. We also appreciate Qian Wang and Long Yuan for their help in conducting the experiments.

Nomenclature

$\Delta\sigma$	Horizontal differential stress, MPa
σ_H	Maximum horizontal stress, MPa
σ_h	Minimum horizontal stress, MPa
σ_V	Overburden stress, MPa
ϕ	Formation porosity, %
I_c	Multiplication coefficient, dimensionless
I_{sw}	Saturation-resistivity increasing coefficient, dimensionless
I_{es}	Stress-resistivity increasing coefficient, dimensionless
K	Side-pressure coefficient, dimensionless
L	Length of rock samples, cm
P_{ef}	Vertical effective stress, MPa
r	Resistance of rock samples, Ω
R_t	Measured resistivity of samples under different stress conditions, Ω·m
R_{tsc}	Corrected resistivity, Ω·m
R_0	Sample resistivity under different confining stress before axial stress is applied, Ω·m
s	Cross section area of samples, cm^2

Appendix

Table A
The variation of resistivity with horizontal differential stress under different minimum horizontal stress values. (explanations: R_t: measured resistivity, Ω·m; $\Delta\sigma$: horizontal differential stress, MPa)

Loading mode	Minimum horizontal stress	Relationship between resistivity and horizontal differential stress	Correlation coefficient
Axial stress is higher than confining stress.	10 MPa	$R_t = 1.1977e^{0.004\Delta\sigma}$	0.9876
	20 MPa	$R_t = 1.1999e^{0.0043\Delta\sigma}$	0.9928
	30 MPa	$R_t = 1.2085e^{0.0045\Delta\sigma}$	0.9985
	40 MPa	$R_t = 1.2183e^{0.0044\Delta\sigma}$	0.9996
	50 MPa	$R_t = 1.2303e^{0.0039\Delta\sigma}$	0.9998
	60 MPa	$R_t = 1.2379e^{0.0041\Delta\sigma}$	0.9999
Confining stress is higher than axial stress.	10 MPa	$R_t = 1.2662e^{0.0047\Delta\sigma}$	0.9407
	20 MPa	$R_t = 1.3244e^{0.0042\Delta\sigma}$	0.9750
	30 MPa	$R_t = 1.3693e^{0.0040\Delta\sigma}$	0.9830
	40 MPa	$R_t = 1.4068e^{0.0038x\Delta\sigma}$	0.9946
	50 MPa	$R_t = 1.4503e^{0.0033x\Delta\sigma}$	0.9987
	60 MPa	$R_t = 1.4800e^{0.0033x\Delta\sigma}$	0.9989

Table B
The variation of resistivity increasing coefficient with horizontal differential stress under different minimum horizontal stress values.

Loading mode	Minimum horizontal stress	Relationship between resistivity increasing coefficient and horizontal differential stress	Correlation coefficient
Axial stress is higher than confining stress	10 MPa	$R_t/R_0 = 1.0215e^{0.0040\Delta\sigma}$	0.9785
	20 MPa	$R_t/R_0 = 1.0095e^{0.0042\Delta\sigma}$	0.9825
	30 MPa	$R_t/R_0 = 1.0017e^{0.0042\Delta\sigma}$	0.9982
	40 MPa	$R_t/R_0 = 1.0011e^{0.0038\Delta\sigma}$	0.9994
	50 MPa	$R_t/R_0 = 1.0002e^{0.0034\Delta\sigma}$	0.9999
	60 MPa	$R_t/R_0 = 1.0000e^{0.0030\Delta\sigma}$	0.9978
Confining stress is higher than axial stress.	10 MPa	$R_t/R_0 = 1.0629e^{0.0047\Delta\sigma}$	0.9785
	20 MPa	$R_t/R_0 = 1.0282e^{0.0043\Delta\sigma}$	0.9733
	30 MPa	$R_t/R_0 = 1.0149e^{0.0040\Delta\sigma}$	0.9968
	40 MPa	$R_t/R_0 = 1.0055e^{0.0038\Delta\sigma}$	0.9961
	50 MPa	$R_t/R_0 = 0.9986e^{0.0034\Delta\sigma}$	0.9926
	60 MPa	$R_t/R_0 = 1.0000e^{0.0030\Delta\sigma}$	0.9985

Table C
The variation of resistivity increasing coefficient with the minimum horizontal stress under different horizontal differential stress values.

Loading mode	Horizontal differential stress	Relationship between resistivity increasing coefficient and minimum horizontal stress	Correlation coefficient
Axial stress is higher than confining stress.	0 MPa	$R_t/R_0 = 1.0010e^{0.0008\sigma h}$	0.9462
	10 MPa	$R_t/R_0 = 0.9970e^{0.0008\sigma h}$	0.9686
	20 MPa	$R_t/R_0 = 0.9940e^{0.0009\sigma h}$	0.9835
	30 MPa	$R_t/R_0 = 0.9922e^{0.0010\sigma h}$	0.9888
	40 MPa	$R_t/R_0 = 0.9918e^{0.0009\sigma h}$	0.9777
	50 MPa	$R_t/R_0 = 0.9900e^{0.0010\sigma h}$	0.9867
Confining stress is higher than axial stress.	0 MPa	$R_t/R_0 = 0.9926e^{0.0038\sigma h}$	0.9454
	10 MPa	$R_t/R_0 = 0.9841e^{0.0022\sigma h}$	0.9855
	20 MPa	$R_t/R_0 = 0.9813e^{0.0019\sigma h}$	0.9999
	30 MPa	$R_t/R_0 = 0.9808e^{0.0017\sigma h}$	0.9811
	40 MPa	$R_t/R_0 = 0.9837e^{0.0015\sigma h}$	0.9656
	50 MPa	$R_t/R_0 = 0.9901e^{0.0010\sigma h}$	0.9986

References

[1] R.C. Glanville, Laboratory study indicates significant effect of pressure on resistivity of reservoir rock, J. Petrol. Technol. 11 (1959) 20–26, https://doi.org/10.2118/1153-G, 04.

[2] P. Glover, R.G. Ross, H. Jolly, The measurement of saturated rock electrical conductivity at lower crustal temperatures and high pressures, High Pres. Res. 5 (1–6) (1990) 705–707, https://doi.org/10.1080/08957959008246233.

[3] W. Jiang, Y. Liu, Study on variation of electrical resistivity under uniaxial pressure environment for rocks, J. Geol. 33 (3) (2009) 299–302.

[4] A. Tinni, C.H. Sondergeld, C.S. Rai, H. Kouam, Effective pressure and microstructure control on resistivity formation factor and seismic waves velocities, in: SPE Annual Technical Conference and Exhibition, vol. 30, 2011, https://doi.org/10.2118/147432-MS. October-2 November, Denver, Colorado, USA.

[5] Y.H. Wang, Y.F. Liu, H.T. Ma, Changing regularity of rock damage variable and resistivity under loading condition, Saf. Sci. 50 (4) (2012) 718–722, https://doi.org/10.1016/j.ssci.2011.08.046.

[6] D. Katsuki, A.N. Tutuncu, Coupling complex resistivity, geomechanical and acoustic properties and permeability in sandstone and shale reservoirs, in: Unconventional Resources Technology Conference, vol. 24, 2017, p. 26, https://doi.org/10.15530/URTEC-2017-2671521. July, Austin, Texas, USA.

[7] B.A. Baldwin, A.A. Chaves, G.A. Latorranca, N.L. Maerefat, B.F. Swanson, Part IV - guidelines for saturating and desaturating core plugs during electrical resistivity measurements; SCA guidelines for sample preparation and porosity measurement of electrical resistivity samples, Log. Anal. 31 (2) (1990) 68–75.

[8] R.J. Evans, J.D. Klein, J.D. Walls, G. White, P.F. Worthington, Part Iii -the mechanics of electrical resistivity measurement on rock samples; SCA guidelines for sample preparation and porosity measurement of electrical resistivity samples, Log. Anal. 31 (2) (1990) 64–67.

[9] S.M. Mahmood, N.L. Maerefat, M.M. Chang, Laboratory measurements of electrical resistivity at reservoir conditions, SPE Form. Eval. 6 (3) (2013) 134–143, https://doi.org/10.2118/18179-PA.

[10] C. Caselle, S. Bonetto, C. Comina, Comparison of laboratory and field electrical resistivity measurements of a gypsum rock for mining prospection applications, International Journal of Mining Science and Technology 29 (6) (2019) 841–849.

[11] W. Wang, H. Xia, Q. Wang, Experimental study of the stress effect on formation resistivity under high temperature and high pressure, Well Logging Technol. 41 (6) (2017) 642–647.

[12] Z. Liu, C. Zhang, G. Zheng, Study on the mechanism of geostress difference effect on tight sandstone resistivity and its correction method, Petrophysics 59 (1) (2018) 1–17, https://doi.org/10.30632/PETRO_059_1_A8.

[13] J. Chen, An efficient layered finite element method with domain decomposition for simulations of resistivity well logging, J. Petrol. Sci. Eng. 150 (2017) 217–223.

[14] J. Zhao, W. Li, C. Xiao, X. Qi, Numerical simulation and correction of electrical resistivity logging for different formation dip angles, J. Petrol. Sci. Eng. 164 (2018) 344–350, https://doi.org/10.1016/j.petrol.2018.01.067.

[15] C. Perez-Rosales, Generalization of the maxwell equation for formation resistivity factors, J. Petrol. Technol. 28 (1976) 819–824, https://doi.org/10.2118/5502-pa, 07.

[16] C. Perez-Rosales, On the relationship between formation resistivity factor and porosity, Int. J. Rock Mech. Min. Sci. Geomech. Abstr. 20 (2) (1982) 531–536, https://doi.org/10.1016/0148-9062(83)90338-8.

[17] M. Küntz, J.C. Mareschal, P. Lavallee, Numerical estimation of electrical conductivity in saturated porous media with 2-D lattice gas, Geophysics 65 (3) (2000) 766–772, https://doi.org/10.1190/1.1444775.

[18] K. Verwer, G.P. Eberli, R.J. Weger, Effect of pore structure on electrical resistivity in carbonates, AAPG (Am. Assoc. Pet. Geol.) Bull. 95 (2) (2011) 175–190, https://doi.org/10.1306/06301010047.

[19] W. Li, C.C. Zou, H. Wang, A model for calculating the formation resistivity factor in low and middle porosity sandstone formations considering the effect of pore geometry, J. Petrol. Sci. Eng. 152 (2017) 193–203.

[20] H. Wang, J. Zhang, The effect of various lengths of pores and throats on the formation resistivity factor, J. Appl. Geophys. 162 (2019) 35–46, https://doi.org/10.1016/j.jappgeo.2019.01.005.

[21] X. Li, W. Zhao, C. Zhou, T. Wang, C. Li, Dual-porosity saturation model of low-porosity and low-permeability clastic reservoirs, Petrol. Explor. Dev. 39 (1) (2012) 88–98, https://doi.org/10.1016/S1876-3804(12)60019-6.